doi:10.1093/brain/awaa180 BRAIN 2020: 143; 2818–2830 | 2818

BRAIN
A JOURNAL OF NEUROLOGY

^{18}F-MK-6240 PET for early and late detection of neurofibrillary tangles

Tharick A. Pascoal,[1,2,3,4,5,6] Joseph Therriault,[1,2,3,4,5] Andrea L. Benedet,[1,2,3,4,5] Melissa Savard,[1,2,3,4,5] Firoza Z. Lussier,[1,2,3,4,5] Mira Chamoun,[1,2,3,4,5] Cécile Tissot,[1,2,3,4,5] Muhammad Naveed Iqbal Qureshi,[1,2,3,4,5] Min Su Kang,[1,2,3,4,5,6] Sulantha Mathotaarachchi,[1,2,3,4,5] Jenna Stevenson,[1,2,3,4,5] Robert Hopewell,[6] Gassan Massarweh,[6] Jean-Paul Soucy,[6] Serge Gauthier[1] and Pedro Rosa-Neto[1,2,3,4,5,6]

See Morén and Varrone (doi:10.1093/brain/awaa220) for a scientific commentary on this article.

Braak stages of tau neurofibrillary tangle accumulation have been incorporated in the criteria for the neuropathological diagnosis of Alzheimer's disease. It is expected that Braak staging using brain imaging can stratify living individuals according to their individual patterns of tau deposition, which may prove crucial for clinical trials and practice. However, previous studies using the first-generation tau PET agents have shown a low sensitivity to detect tau pathology in areas corresponding to early Braak histopathological stages (~20% of cognitively unimpaired elderly with tau deposition in regions corresponding to Braak I–II), in contrast to ~80–90% reported in post-mortem cohorts. Here, we tested whether the novel high affinity tau tangles tracer ^{18}F-MK-6240 can better identify individuals in the early stages of tau accumulation. To this end, we studied 301 individuals (30 cognitively unimpaired young, 138 cognitively unimpaired elderly, 67 with mild cognitive impairment, 54 with Alzheimer's disease dementia, and 12 with frontotemporal dementia) with amyloid-β ^{18}F-NAV4694, tau ^{18}F-MK-6240, MRI, and clinical assessments. ^{18}F-MK-6240 standardized uptake value ratio images were acquired at 90–110 min after the tracer injection. ^{18}F-MK-6240 discriminated Alzheimer's disease dementia from mild cognitive impairment and frontotemporal dementia with high accuracy (~85–100%). ^{18}F-MK-6240 recapitulated topographical patterns consistent with the six hierarchical stages proposed by Braak in 98% of our population. Cognition and amyloid-β status explained most of the Braak stages variance ($P < 0.0001$, $R^2 = 0.75$). No single region of interest standardized uptake value ratio accurately segregated individuals into the six topographic Braak stages. Sixty-eight per cent of the cognitively unimpaired elderly amyloid-β-positive and 37% of the cognitively unimpaired elderly amyloid-β-negative subjects displayed tau deposition, at least in the transentorhinal cortex (Braak I). Tau deposition solely in the transentorhinal cortex was associated with an elevated prevalence of amyloid-β, neurodegeneration, and cognitive impairment ($P < 0.0001$). ^{18}F-MK-6240 deposition in regions corresponding to Braak IV–VI was associated with the highest prevalence of neurodegeneration, whereas in Braak V–VI regions with the highest prevalence of cognitive impairment. Our results suggest that the hierarchical six-stage Braak model using ^{18}F-MK-6240 imaging provides an index of early and late tau accumulation as well as disease stage in preclinical and symptomatic individuals. Tau PET Braak staging using high affinity tracers has the potential to be incorporated in the diagnosis of living patients with Alzheimer's disease in the near future.

1 Translational Neuroimaging Laboratory, The McGill University Research Centre for Studies in Aging, Alzheimer's Disease ResearchUnit, McGill University, Montreal, Canada
2 Douglas Research Institute, Le Centre intégré universitaire de santé et de services sociaux (CIUSSS) de l'Ouest-de-l'Île-de-Montréal, McGill University, Montreal, Canada
3 Department of Neurology and Neurosurgery, McGill University, Montreal, Canada
4 Department of Psychiatry, McGill University, Montreal, Canada
5 Department of Pharmacology and Therapeutics, McGill University, Montreal, Canada
6 Montreal Neurological Institute, McGill University, Montreal, QC, Canada

Received January 29, 2020. Revised March 30, 2020. Accepted April 14, 2020. Advance access publication July 16, 2020

Braak stages of tau neurofibrillary tangle accumulation have been incorporated in the criteria for the neuropathological diagnosis of Alzheimer's disease. It is expected that Braak staging using brain imaging can stratify living individuals according to their individual patterns of tau deposition, which may prove crucial for clinical trials and practice. However, previous studies using the first-generation tau PET agents have shown a low sensitivity to detect tau pathology in areas corresponding to early Braak histopathological stages (~20% of cognitively unimpaired elderly with tau deposition in regions corresponding to Braak I–II), in contrast to ~80–90% reported in post-mortem cohorts. Here, we tested whether the novel high affinity tau tangles tracer ^{18}F-MK-6240 can better identify individuals in the early stages of tau accumulation. To this end, we studied 301 individuals (30 cognitively unimpaired young, 138 cognitively unimpaired elderly, 67 with mild cognitive impairment, 54 with Alzheimer's disease dementia, and 12 with frontotemporal dementia) with amyloid-β ^{18}F-NAV4694, tau ^{18}F-MK-6240, MRI, and clinical assessments. ^{18}F-MK-6240 standardized uptake value ratio images were acquired at 90–110 min after the tracer injection. ^{18}F-MK-6240 discriminated Alzheimer's disease dementia from mild cognitive impairment and frontotemporal dementia with high accuracy (~85–100%). ^{18}F-MK-6240 recapitulated topographical patterns consistent with the six hierarchical stages proposed by Braak in 98% of our population. Cognition and amyloid-β status explained most of the Braak stages variance ($P < 0.0001$, $R^2 = 0.75$). No single region of interest standardized uptake value ratio accurately segregated individuals into the six topographic Braak stages. Sixty-eight per cent of the cognitively unimpaired elderly amyloid-β-positive and 37% of the cognitively unimpaired elderly amyloid-β-negative subjects displayed tau deposition, at least in the transentorhinal cortex (Braak I). Tau deposition solely in the transentorhinal cortex was associated with an elevated prevalence of amyloid-β, neurodegeneration, and cognitive impairment ($P < 0.0001$). ^{18}F-MK-6240 deposition in regions corresponding to Braak IV–VI was associated with the highest prevalence of neurodegeneration, whereas in Braak V–VI regions with the highest prevalence of cognitive impairment. Our results suggest that the hierarchical six-stage Braak model using ^{18}F-MK-6240 imaging provides an index of early and late tau accumulation as well as disease stage in preclinical and symptomatic individuals. Tau PET Braak staging using high affinity tracers has the potential to be incorporated in the diagnosis of living patients with Alzheimer's disease in the near future.

1 Translational Neuroimaging Laboratory, The McGill University Research Centre for Studies in Aging, Alzheimer's Disease ResearchUnit, McGill University, Montreal, Canada
2 Douglas Research Institute, Le Centre intégré universitaire de santé et de services sociaux (CIUSSS) de l'Ouest-de-l'Île-de-Montréal, McGill University, Montreal, Canada
3 Department of Neurology and Neurosurgery, McGill University, Montreal, Canada
4 Department of Psychiatry, McGill University, Montreal, Canada
5 Department of Pharmacology and Therapeutics, McGill University, Montreal, Canada
6 Montreal Neurological Institute, McGill University, Montreal, QC, Canada

Correspondence to: Pedro Rosa-Neto, MD, PhD
The McGill University Research Centre for Studies in Aging
Douglas Hospital, 6825 La Salle Blvd - Montreal, QC, Canada H4H 1R3
E-mail: pedro.rosa@mcgill.ca

Keywords: neurofibrillary tangles; Braak stages; Alzheimer's disease; positron emission tomography

Abbreviations: CDR = Clinical Dementia Rating; MCI = mild cognitive impairment; MMSE = Mini-Mental State Examination; SUVR = standardized uptake value ratio

Introduction

Post-mortem studies suggest that the accumulation of tau neurofibrillary tangles in Alzheimer's disease follows a stereotypical pattern that begins in the transentorhinal cortex, spreading to the entorhinal and hippocampal cortices, laterally in the temporal lobe, finally reaching association and primary sensory cortices (Braak and Braak, 1991, 1997; Braak *et al.*, 2006, 2011). This pattern of tau propagation—known as Braak stages—is closely related to other aspects of Alzheimer's disease pathophysiology, such as amyloid-β, neuronal injury, and cognitive impairment (Braak and Braak, 1991; Alafuzoff *et al.*, 2008). Thus, Braak staging was incorporated in the neuropathological diagnosis criteria of Alzheimer's disease (Hyman *et al.*, 2012; Montine *et al.*, 2012). It is postulated that *in vivo* Braak staging has the potential to stratify patients according to their brain patterns of tau propagation, offering information on the patients' tau pathology and disease stage, which may prove to be critical for clinical trials and practice. For instance, accurate *in vivo* tau staging may have immediate applications in anti-tau clinical trials, as individuals may show inherently different regional rates of tau deposition depending on their initial stage

of tau accumulation, which may bias the quantification of possible drug effects on tau pathology over time.

In vivo studies using the first-generation tau PET tracers have shown high performance for the diagnosis of Alzheimer's disease dementia and patterns of tracer uptake that resemble those observed in post-mortem studies (Chien *et al.*, 2013; Maruyama *et al.*, 2013; Villemagne and Okamura, 2014; Harada *et al.*, 2015; Kimura *et al.*, 2015; Gordon *et al.*, 2016; Johnson *et al.*, 2016; Scholl *et al.*, 2016; Pontecorvo *et al.*, 2017; Lowe *et al.*, 2018). However, off-target binding may heavily influence the signal of some of these tau tracers in regions considered to be target for Alzheimer's disease. For example, ^{18}F-THK5351 uptake is driven by monoamine oxidase B availability in regions including the cingulate and temporoparietal cortices (Ng *et al.*, 2017). ^{11}C-PBB3 may bind to α-synuclein (Koga *et al.*, 2017), whereas ^{18}F-flortaucipir uptake may be influenced by monoamine oxidase A (Hostetler *et al.*, 2016) Although several studies have reported that ^{18}F-flortaucipir shows excellent performance for depict tau pathology in regions comprising late Braak stages (Chien *et al.*, 2013; Gordon *et al.*, 2016; Johnson *et al.*, 2016; Scholl *et al.*, 2016; Pontecorvo *et al.*, 2017; Lowe *et al.*, 2018), its performance for early tau stages remains elusive. For example, abnormal ^{18}F-flortaucipir uptake has been reported in only ∼10% and ∼30% of cognitively unimpaired elderly amyloid-β-negative and -positive subjects (Schwarz *et al.*, 2016; Pontecorvo *et al.*, 2017; Lowe *et al.*, 2018), respectively, in contrast to post-mortem studies suggesting tau abnormalities in 80–90% of the elderly populations (Braak and Braak, 1997; Guillozet *et al.*, 2003). Also, these studies suggest that cognitive performance and amyloid-β deposition explain only ∼20% of the ^{18}F-flortaucipir Braak staging variance (Schwarz *et al.*, 2016), suggesting a weak association between Braak stages and the other key Alzheimer's disease-related processes. Indeed, a recent *in vivo* autopsy study established that ^{18}F-flortaucipir uptake accurately concords only with Braak stage IV or greater (Lowe *et al.*, 2020). This reduced sensitivity to quantify early Braak stages may be related to the relatively low affinity of ^{18}F-flortaucipir for tau tangles (dissociation constant ∼14.6 nM) (Xia *et al.*, 2013). A recent study suggested ^{18}F-MK-6240 as a promising biomarker for detecting tau tangles in a middle-aged cohort of cognitively unimpaired individuals (Betthauser *et al.*, 2020). Here, we tested whether the novel subnanomolar affinity tau tangles tracer ^{18}F-MK-6240 (dissociation constant ∼0.3 nM) is able to recapitulate early and late Braak histopathological stages in living humans (Hostetler *et al.*, 2016; Pascoal *et al.*, 2018*b*; Betthauser *et al.*, 2019; Lohith *et al.*, 2019). Because of its higher affinity to tau tangles, we hypothesize that ^{18}F-MK-6240 will capture early tau stages and a strong association between tau stages with amyloid-β status and cognitive deficits, as previously described in histopathological cohorts (Braak and Braak, 1991, 1997; Braak *et al.*, 2006, 2011).

Materials and methods

Participants

Study participants from the community or outpatients at the McGill University Research Centre for Studies in Aging were enrolled in the Translational Biomarkers of Aging and Dementia (TRIAD) cohort, McGill University, Canada. The cohort participants had a detailed clinical assessment, including the Clinical Dementia Rating (CDR) and Mini-Mental State Examination (MMSE). Cognitively unimpaired participants had no objective cognitive impairment and a CDR score of 0. Mild cognitive impairment (MCI) individuals had subjective and objective cognitive impairments, preserved activities of daily living, and a CDR score of 0.5. Patients with mild-to-moderate sporadic Alzheimer's disease dementia had a CDR score between 0.5 and 2, and met the National Institute on Aging and the Alzheimer's Association criteria for probable Alzheimer's disease determined by a physician (McKhann *et al.*, 2011). Sporadic early-onset Alzheimer's disease dementia were individuals with dementia onset before 65 years (Snowden *et al.*, 2011). Frontotemporal dementia patients had a clinical diagnosis of behaviour or semantic frontotemporal dementia variant and were amyloid-β PET negative (Neary *et al.*, 2005). Of 12 patients with frontotemporal dementia, two had a microtubule-associated protein tau mutation (P301L) (Heutink, 2000), which is most often associated with 4 repeats (4R) tau isoform in humans, one had a progranulin mutation, and nine were sporadic. Participants were excluded if they had inadequately treated conditions, active substance abuse, recent head trauma, or major surgery, or if they had MRI/PET safety contraindication. Alzheimer's disease patients did not discontinue medications for this study. This study was approved by the Douglas Mental Health University Institute Research Ethics Board and Montreal Neurological Instituted PET working committee, and written informed consent was obtained from all participants.

Imaging

All individuals had a 3D T_1-weighted MRI (3 T Siemens) and ^{18}F-AZD4694 and ^{18}F-MK-6240 PET scans acquired with a brain-dedicated Siemens High Resolution Research Tomograph in the Montreal Neurological Institute. Tau tangle ^{18}F-MK-6240 images were acquired at 90–110 min after the intravenous bolus injection of the tracer and were reconstructed using an OSEM algorithm on a 4D volume with four frames (4 × 300 s) (Pascoal *et al.*, 2018*b*). Amyloid-β ^{18}F-AZD4694 images were acquired at 40–70 min after the intravenous bolus injection of the tracer, and scans were reconstructed with the same OSEM algorithm on a 4D volume with three frames (3 × 600 s) (Cselenyi *et al.*, 2012). At the end of each PET acquisition, a 6-min transmission scan was conducted with a rotating ^{137}Cs point source for attenuation correction. The images were additionally corrected for motion, dead time, decay, and random and scattered coincidences. Briefly, T_1-weighted MRIs were non-uniformity and field distortions corrected. PET images were then automatically registered to T_1-weighted image space, and the T_1-weighted images were linearly and non-linearly registered to the MNI reference space (Mazziotta *et al.*, 1995). PET images were meninges and skull stripped and non-linearly registered to the MNI space using the transformations from the T_1-weighted image to MNI

space and from the PET image to T_1-weighted image space. ^{18}F-MK-6240 standardized uptake value ratio (SUVR) and ^{18}F-AZD4694 SUVR used the inferior cerebellum and whole cerebellum grey matter as the reference region, respectively (Cselenyi *et al.*, 2012; Pascoal *et al.*, 2018*b*). PET images were spatially smoothed to achieve a final 8-mm full-width at half-maximum resolution. Amyloid-β ^{18}F-AZD4694 positivity was determined visually by the consensus of two neurologists blinded to the diagnosis. Global ^{18}F-AZD4694 SUVR values were estimated from the precuneus, prefrontal, orbitofrontal, parietal, temporal, and cingulate cortices (Pascoal *et al.*, 2018*a*). Hippocampal volume was measured with Freesurfer version 6.0 using the Desikan-Killiany-Tourville grey matter parcellation (Klein and Tourville, 2012). We also used the Desikan-Killiany-Tourville atlas to define regions of interest (Klein and Tourville, 2012). The transentorhinal cortex was defined in stereotaxic space based on established segmentation procedures on a 1-mm isotropic voxel matrix (Tward *et al.*, 2017; Kulason *et al.*, 2019). Braak stages were based on the anatomical brain regions proposed by Braak (Braak and Braak, 1991, 1997; Braak *et al.*, 2006; Braak *et al.*, 2011) as follows: Braak I (transentorhinal), Braak II (entorhinal and hippocampus), Braak III (amygdala, parahippocampal gyrus, fusiform gyrus, lingual gyrus), Braak IV (insula, inferior temporal, lateral temporal, posterior cingulate, and inferior parietal), Braak V (orbitofrontal, superior temporal, inferior frontal, cuneus, anterior cingulate, supramarginal gyrus, lateral occipital, precuneus, superior parietal, superior frontal, rostro medial frontal), and Braak VI (paracentral, postcentral, precentral, and pericalcarine). An automatic pipeline was developed to determine the individuals' Braak stages in a hierarchical fashion, where later stages can only be achieved if the individual is positive for the previous stages; otherwise the participant was considered Braak stages discordant.

Statistical methods

Statistical analyses were performed using R statistical software version 3.1.2 (http://www.r-project.org/); voxel-wise statistics were performed using MATLAB software version 9.2 (http://www.mathworks.com) with VoxelStats package (Mathotaarachchi *et al.*, 2016). Regressions tested demographic differences between groups for continuous variables, whereas chi-square was used for categorical variables. We showed diagnosis-associated PET abnormalities using voxel-wise mean and standard deviation parametric maps. Voxel-wise receiver operating characteristic curves contrasting groups provided the area under the curve for disease diagnosis or biomarkers positivity. We tested the associations between biomarkers using linear regressions adjusted for age, sex, years of education, and apolipoprotein E4 (APOE ε4) carriage status. Tau positivity was defined as 2.5 standard deviations (SD) higher than the mean SUVR of cognitively unimpaired young individuals for each respective region of interest. Tau cut-off values were also assessed using Gaussian mixture model. The presence of abnormally reduced hippocampal volume was defined as 2.5 SD smaller than the average volume of cognitively unimpaired young individuals after correction for intracranial volume. To create the voxel-wise frequency of tau positivity maps, first, we calculated z-score parametric maps for each subject, anchored on the normative data of the cognitively unimpaired young population. Then, we generated binary maps of tau positivity for each individual as 2.5 SD higher than the mean SUVR of cognitively unimpaired young and averaged these maps. The relationships between Braak stages (seven classes, Braak 0–VI) and clinical diagnosis, cognition, amyloid-β, and hippocampal volume were assessed using ordinal logistic regression analysis controlling for age and gender. The models were evaluated using estimated *P*-value and entropy R^2. Entropy R^2 estimates the goodness-of-fit of logistic regression models.

Data availability

The data presented in this study are available from the corresponding author on request. The data are not publicly available due to their containing information that could compromise the privacy of research participants.

Results

Participants

We studied 301 individuals [30 cognitively unimpaired young, 138 cognitively unimpaired elderly (27% amyloid-β+), 67 MCI (61% amyloid-β+), 30 early-onset Alzheimer's disease dementia and 21 late-onset Alzheimer's disease dementia (100% amyloid-β+), three individuals had a clinical diagnosis of Alzheimer's disease dementia but were amyloid-β– (100% amyloid-β–), and 12 frontotemporal dementia patients (100% amyloid-β–)]. We define as 'neurofibrillary tangle predominant dementia' the three individuals who had a clinical diagnosis of Alzheimer's disease dementia and *in vivo* PET suggesting scarce amyloid-β pathology (amyloid-β–) and high neocortical levels of tau tangles. Amyloid-β and tau PET images of the individuals with neurofibrillary tangle predominant dementia are presented in Supplementary Fig. 1. Table 1 presents the demographic characteristics of the population.

Diagnosis effect on ^{18}F-MK-6240 uptake

Voxel-wise ^{18}F-MK-6240 SUVR mean maps showed visually higher uptake in Alzheimer's disease dementia and MCI than in cognitively unimpaired and frontotemporal dementia cases (Fig. 1). ^{18}F-MK-6240 standard deviation maps revealed that the cognitively unimpaired amyloid-β– group had the highest uptake variability in the transentorhinal/entorhinal cortex. The cognitively unimpaired amyloid-β+ group had the highest uptake variability in the mediobasal temporal, MCI amyloid-β– in the lateral temporal, and MCI amyloid-β+ in the temporal, posterior cingulate, and precuneus cortices. The Alzheimer's disease dementia group had the highest uptake variability in the posterior cingulate/precuneus cortices. Cognitively unimpaired young and frontotemporal dementia groups had homogeneous ^{18}F-MK-6240 uptake across the cortex (Fig. 1).

Table 1 Demographics and characteristics of the population

Characteristics	Young Amyloid-β–	Elderly Amyloid-β–	Elderly Amyloid-β+	MCI Amyloid-β–	MCI Amyloid-β+	EOAD Amyloid-β+	LOAD Amyloid-β+	NTPD [h]Amyloid-β–	FTD Amyloid-β–	*P*-value
n	30	101	37	26	41	30	21	3	12	–
Age, years, mean (SD)	22.2 (1.3)	69.6 (7.6)[a]	74.9 (5.1)[a,b,e,g]	70.7 (11.2)[a,e,g]	72 (7.5)[a,e,g]	59.6 (5.7)[a,b]	75.7 (6.2)[a,b,e,g]	68.3 (2.9)*	59.3 (7.4)[a,b]	<0.0001
Male, *n* (%)	11 (37)	39 (39)	8 (22)	17 (65)[c]	20 (49)[c]	14 (47)[c]	8 (38)	1 (33)*	5 (42)	0.049
Education, years, mean (SD)	16.3 (1.4)	15.8 (3.9)	14.4 (3.3)	14 (4.7)	15.5 (3.6)	14.5 (3.4)	14.3 (4.8)	12 (2)*	13 (4.2)	0.034
MMSE score, mean (SD)	29.8 (0.48)	29.1 (1.15)	29 (0.9)[e–g]	27.2 (1.9)[a,e–g]	27.6 (2)[a,e–g]	16.8 (6.6)[a,b,g]	21.2 (5.3)[a,b,e]	22.6 (3.5)*	23.5 (8.2)[a,b]	<0.0001
APOE ε4, *n* (%)	7 (23)	28 (28)	11 (30)[e]	6 (23)[d,e]	21 (51)[a,b,g]	19 (63)[a,b,g]	10 (48)	0 (0)*	1 (8)	0.001
^{18}F-MK-6240 SUVR Braak I, mean (SD)	0.98 (0.07)	1.13 (0.17)	1.35 (0.34)[d–f]	1.29 (0.69)[d–f]	2.22 (0.7)[a,b,e–g]	2.75 (0.9)[a,b,g]	3.05 (1.32)[a,b,g]	3.21 (0.43)*	0.96 (0.1)	<0.0001
^{18}F-MK-6240 SUVR Braak II, mean (SD)	1 (0.09)	1.14 (0.15)	1.33 (0.26)[d–f]	1.27 (0.53)[d–f]	2.03 (0.56)[a,b,e–g]	2.42 (0.7)[a,b,g]	2.6 (0.97)[a,b,g]	2.58 (0.41)*	0.97 (0.1)	<0.0001
^{18}F-MK-6240 SUVR Braak III, mean (SD)	1.32 (0.09)	1.36 (0.1)	1.44 (0.18)[d–f]	1.51 (0.68)[d–f]	1.87 (0.47)[a,b,e–g]	3.4 (1.05)[a,b,g]	2.6 (0.9)[a,b,e,g]	3.39 (0.29)*	1.25 (0.13)	<0.0001
^{18}F-MK-6240 SUVR Braak IV, mean (SD)	1.14 (0.10)	1.17 (0.1)	1.24 (0.16)[d–f]	1.37 (0.89)[d–f]	1.8 (0.6)[a,b,e–g]	3.4 (1.2)[a,b,g]	2.6 (1.18)[a,b,e,g]	3.98 (0.19)*	1.09 (0.11)	<0.0001
^{18}F-MK-6240 SUVR Braak V, mean (SD)	1.26 (0.12)	1.23 (0.12)	1.26 (0.12)[d–f]	1.38 (0.6)[e,f]	1.66 (0.42)[b,e,f]	3.7 (1.3)[a,b,g]	2.4 (1.02)[a,b,e,g]	3.6 (0.37)*	1.16 (0.12)	<0.0001
^{18}F-MK-6240 SUVR Braak VI, mean (SD)	1.37 (0.13)	1.32 (0.13)	1.33 (0.12)[e,f]	1.41 (0.36)[e,f]	1.56 (0.28)[e,f]	3.2 (1.21)[a,b,b]	2.13 (0.91)[a,b,e,g]	2.6 (0.22)*	1.23 (0.13)	<0.0001

P-values indicate the results of the analysis of variance to assesses difference between groups except for gender and *APOE* ε4 status where a contingency chi-square was performed. Tukey's *post hoc* analysis tested significant differences from: [a]Young; [b]Elderly amyloid-β–; [c]Elderly amyloid-β+; [d]MCI amyloid-β+; [e]EOAD; [f]LOAD; and [g]FTD.

[h]Neurofibrillary tangle predominant dementia (NTPD) were individuals with a clinical diagnosis of dementia and *in vivo* PET biomarkers suggesting high neocortical levels of tau tangle pathology and scarce amyloid pathology (amyloid-β–).

*No statistical analysis was performed for the NTPD group due to the small number of subjects. Elderly = cognitively unimpaired elderly; EOAD = early-onset Alzheimer's disease dementia; FTD = frontotemporal dementia; LOAD = late onset Alzheimer's disease dementia; Young = cognitively unimpaired young.

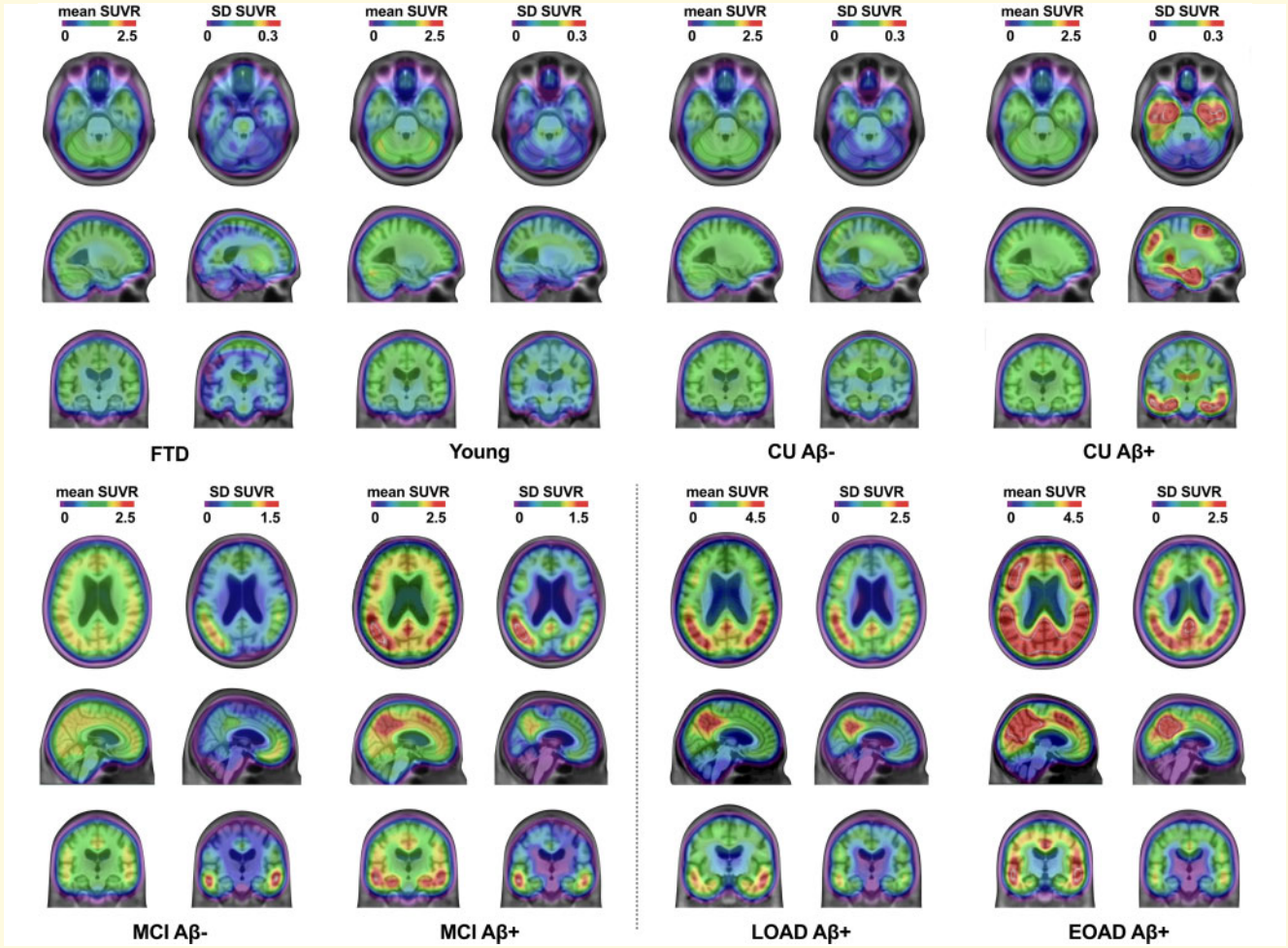

Figure 1 ^{18}F-MK-6240 SUVR average and standard deviation parametric maps in clinical groups segregated by amyloid-β status. The figure shows the mean and the standard deviation (SD) of ^{18}F-MK-6240 parametric SUVR maps across groups. Aβ = amyloid-β; CU = cognitively unimpaired; EOAD = early-onset Alzheimer's disease dementia; FTD = frontotemporal dementia; LOAD = late onset Alzheimer's disease dementia.

^{18}F-MK-6240 shows high performance for the diagnosis of Alzheimer's disease

Voxel-wise receiver operating characteristic curves revealed that ^{18}F-MK-6240 SUVR showed high performance in differentiating Alzheimer's disease dementia from cognitively unimpaired and frontotemporal dementia patients (area under the curve ∼90–100%) across the whole brain cortex (Fig. 2). ^{18}F-MK-6240 uptake differentiated MCI amyloid-β+ from cognitively unimpaired and frontotemporal dementia with the highest accuracy in the medial temporal structures (area under the curve ∼90–100%) ^{18}F-MK-6240 SUVR in the transentorhinal, entorhinal, and hippocampal cortices discriminated cognitively unimpaired amyloid-β– from cognitively unimpaired amyloid-β+ (area under the curve ∼80%) with the highest accuracy (Fig. 2).

^{18}F-MK-6240 is associated with amyloid-β, hippocampal volume, and cognition

Across the entire population, ^{18}F-MK-6240 uptake was positively associated with amyloid-β ^{18}F-AZD4694 uptake (Fig. 3A) and negatively associated with hippocampal volume (Fig. 3B) and general cognitive performance (MMSE score) (Fig. 3C). The association between ^{18}F-MK-6240 and ^{18}F-AZD4694 uptake and hippocampal volume was stronger in early Braak stages (Braak I–IV), whereas the association between ^{18}F-MK-6240 and cognition was stronger in later stages (Braak V–VI).

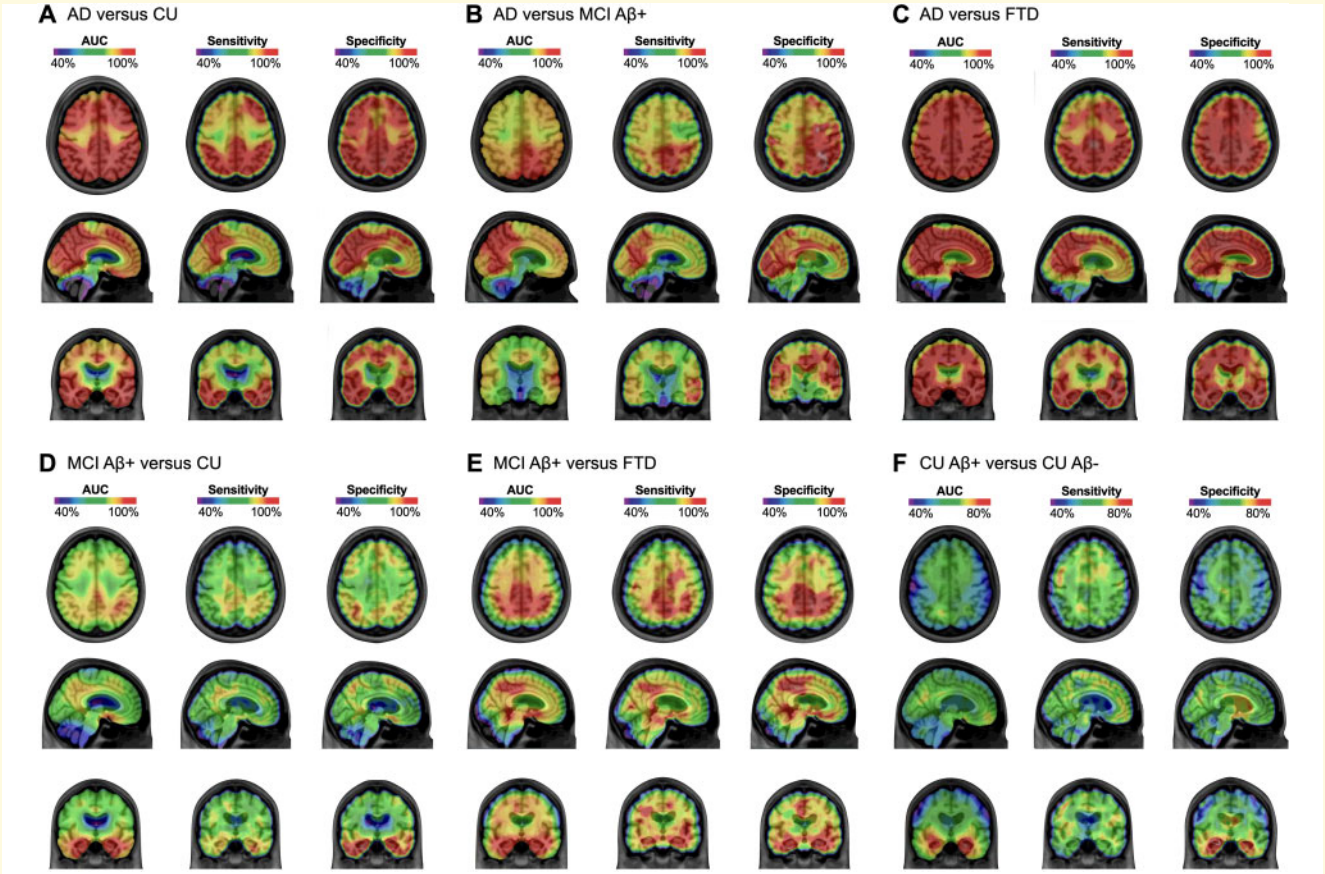

Figure 2 ^{18}F-MK-6240 shows high performance for the diagnosis of Alzheimer's disease. The figure shows voxel-wise area under the curve (AUC), sensitivity, and specificity maps obtained from receiver operating characteristic curves performed between groups. Aβ = amyloid-β; AD = Alzheimer's disease dementia; CU = cognitively unimpaired; FTD = frontotemporal dementia.

^{18}F-MK-6240 recapitulates the hierarchical six-stage Braak model

Using cut-off values to indicate ^{18}F-MK-6240 SUVR positivity defined as 2.5 SD greater than mean of the young controls applied to the elderly population (cognitively unimpaired, MCI, and Alzheimer's disease dementia), ^{18}F-MK-6240 SUVR positivity was more frequent in regions of interest in the transentorhinal (63%), followed by the entorhinal (58%), hippocampus (55%), and amygdala (54%) (Fig. 4). The regions showing the lowest prevalence of tau positivity were the paracentral, precentral, and postcentral cortices (~20%). ^{18}F-MK-6240 positivity was more frequent in Braak I (63%), followed by Braak II (56%), III (40%), IV (30%), V (25%), and VI (20%) regions, supporting that ^{18}F-MK-6240 deposition starts in Braak I and has its last stage in Braak VI (Fig. 4).

The cut-off values indicating ^{18}F-MK-6240 SUVR positivity in regions corresponding to Braak stages were: Braak I = 1.16, Braak II = 1.23, Braak III = 1.55, Braak IV = 1.39, Braak V = 1.56, and Braak VI = 1.7 (Fig. 5A). Similar cut-off values were obtained using Gaussian mixture model (Supplementary Fig. 2). Using the cut-offs mentioned above, 98% of our populations followed the six Braak stages model (seven classes, Braak 0–VI) in a hierarchical manner (i.e. later stages can only be achieved if the individuals is positive for the previous stages; otherwise the individual was considered Braak stages discordant) (Fig. 5B). All six discordant individuals (two cognitively unimpaired, two MCI, and two early-onset Alzheimer's disease dementia) spared tau deposition in temporal structures, three spared Braak I and II, two spared only Braak II, and one spared Braak III region. Five individuals were Braak VI but amyloid-β– [two MCI and three dementia (neurofibrillary tangle predominant dementia)]. Stratified analysis by clinical diagnosis revealed that all cognitively unimpaired young and frontotemporal dementia individuals were amyloid-β– and tau–; 37% of cognitively unimpaired amyloid-β– were tau+; 40% of MCI amyloid-β– were tau+; 68% of cognitively unimpaired amyloid-β+ were tau+; 88% of MCI amyloid-β+ were tau+; 100% of early- and late-onset Alzheimer's disease dementia were tau+; and 100% of neurofibrillary tangles predominant dementia individuals were tau+, at least in the transentorhinal cortex (Fig. 5C). Stratifications using a four-class Braak model (i.e. Braak 0, I/II, III/IV, and V/VI) provided a similar number of

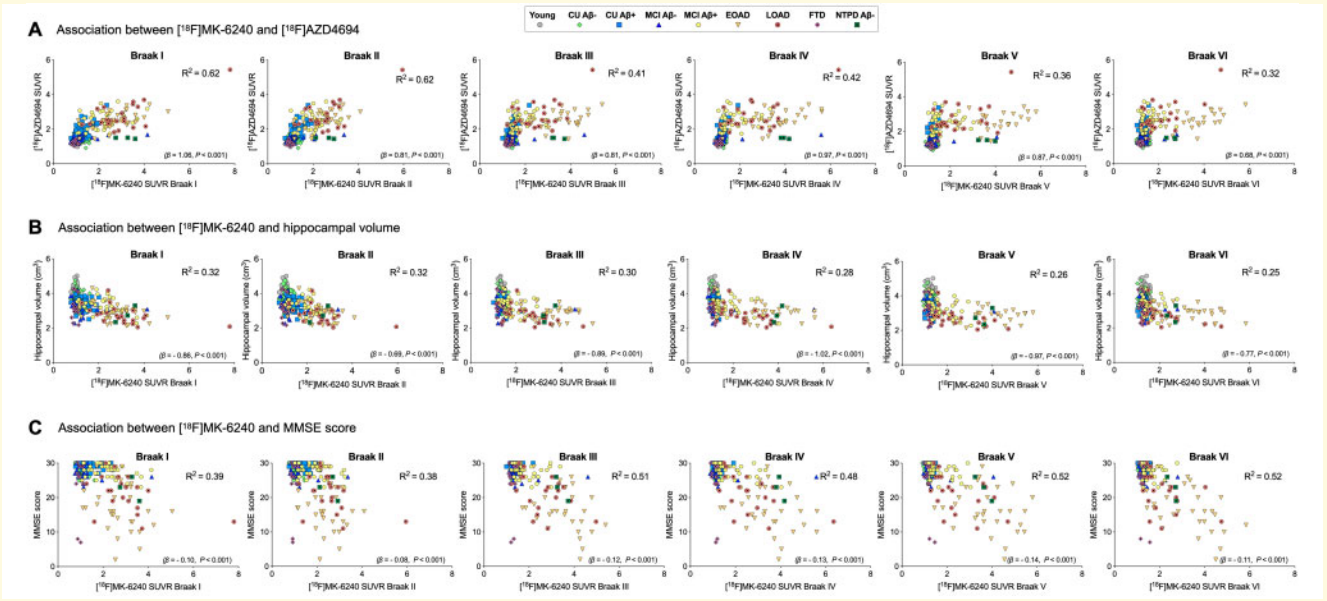

Figure 3 ^{18}F-MK-6240 SUVR is associated with amyloid-β deposition, hippocampal volume, and cognition. (**A**–**C**) The association between ^{18}F-MK-6240 SUVR and global amyloid-β ^{18}F-AZD4694 SUVR, hippocampal volume, and general cognition (MMSE score), respectively. The linear regression models were adjusted for age, sex, years of education, and APOE ε4 carriage status. Associations involving hippocampal volume were further corrected for intracranial volume. Aβ = amyloid-β; Elderly = cognitively unimpaired elderly; EOAD = early-onset Alzheimer's disease dementia; FTD = frontotemporal dementia; LOAD = late onset Alzheimer's disease dementia; NTPD = neurofibrillary tangle predominant dementia; Young = cognitively unimpaired (CU) young.

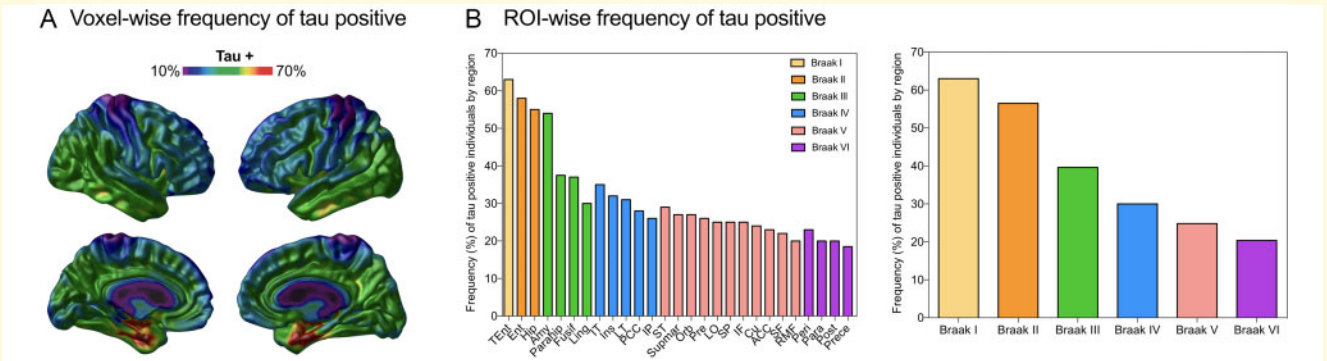

Figure 4 ^{18}F-MK-6240 accumulation hierarchically follows the six Braak stages. (**A**) A map superimposed on a structural magnetic resonance template, showing the frequency of tau positivity in all brain voxel in the elderly population (cognitively unimpaired, MCI, and Alzheimer's disease dementia). (**B**) The frequency of tau positive individuals in anatomically segregated regions (*left*) and Braak regions (*right*) in the elderly. ACC = anterior cingulate; Amy = amygdala; Cu = cuneus; Ent = entorhinal; Fusif = fusiform gyrus; Hip = hippocampus; IF = inferior frontal; Ins = insula; IP = inferior parietal; IT = inferior temporal; Ling = lingual gyrus; LO = lateral occipital; LT = lateral temporal; Orb = orbitofrontal; Para = paracentral; Parahip = parahippocampal gyrus; PCC = posterior cingulate; Peri = pericalcarine; Post = postcentral; Pre = precuneus; Prece = precentral; RMF = rostro medial frontal; ROI = region of interest; SF = superior frontal; SP = superior parietal; ST = superior temporal; Supmar = supramarginal gyrus; TEnt = transentorhinal.

non-zero Braak stage individuals than the seven-class model (Supplementary Fig. 3).

Stratified analysis by Braak stages in individuals in the Alzheimer's disease spectrum (cognitively unimpaired elderly, MCI amyloid-β+, and Alzheimer's disease dementia amyloid-β+) revealed an increased prevalence of amyloid-β deposition, neurodegeneration, and cognitive symptoms in individuals Braak stage I (Table 2). We also found that the prevalence of neurodegeneration reached a plateau in Braak IV, whereas Braak stages V–VI were invariably associated with impaired cognition (Table 2). Ordinal logistic regression analysis revealed that the ^{18}F-MK-6240 six-stage Braak

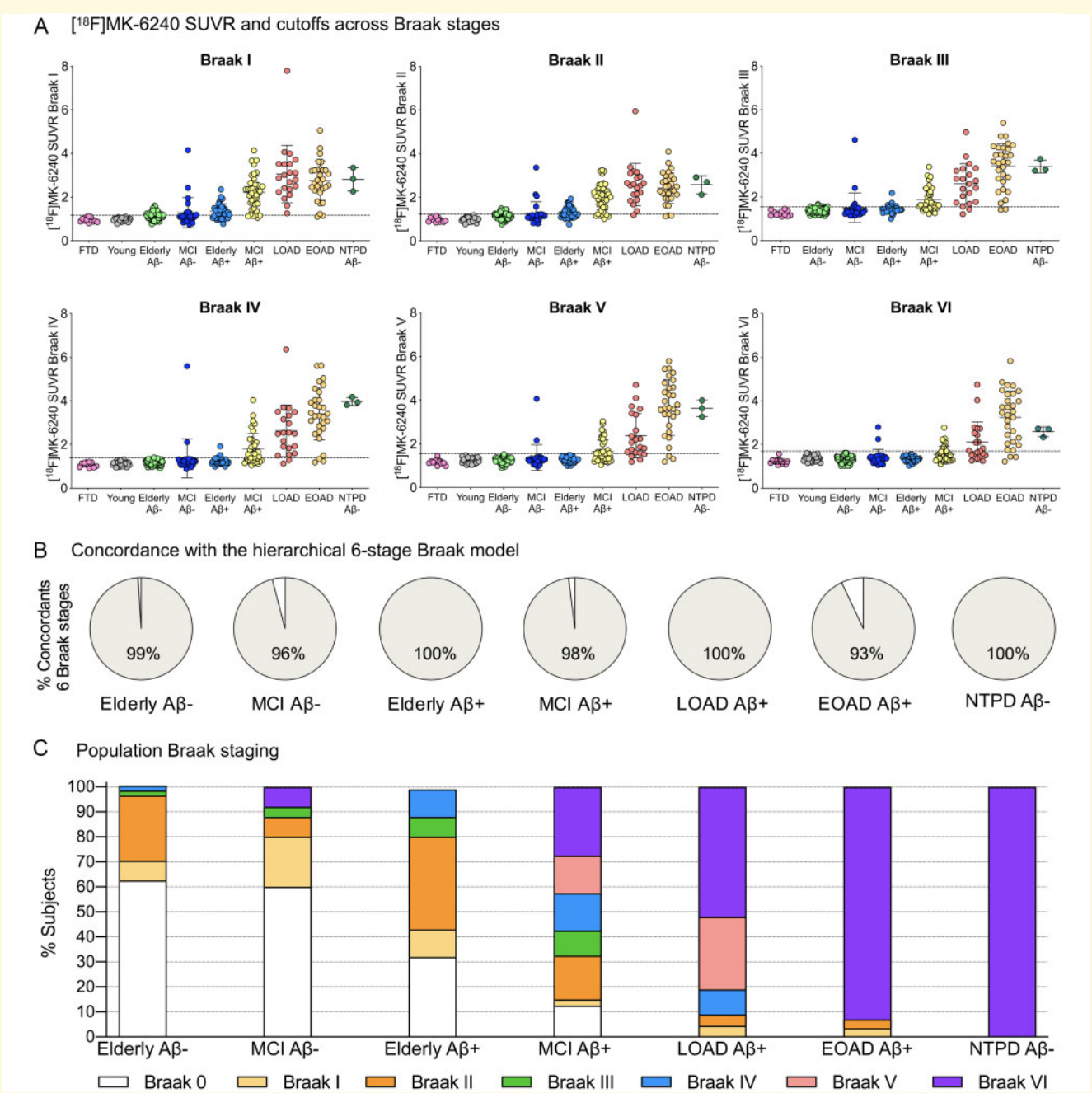

Figure 5 ^{18}F-MK-6240 SUVR uptake recapitulates the six-stage Braak model. (**A**) ^{18}F-MK-6240 SUVR distribution across diagnostic groups and Braak stages. Dashed lines show cut-off values of ^{18}F-MK-6240 SUVR positivity for each Braak stage: Braak I = 1.16, Braak II = 1.23, Braak III = 1.55, Braak IV = 1.39, Braak V = 1.56, and Braak VI = 1.7. (**B**) Percentage of individuals that followed the six Braak stages hierarchically (i.e. later stages can only be achieved if positive for previous stages; otherwise the individual was considered Braak stage discordant). (**C**) The Braak stage distributions across groups [elderly amyloid-β– (n = 101), MCI amyloid-β– (n = 26), elderly amyloid-β+ (n = 37), MCI amyloid-β+ (n = 41), LOAD amyloid-β+ (n = 30), LOAD amyloid-β+ (n = 21), NTPD (n = 3)]. Individuals in Braak stage 0 were tau negative in all Braak regions. Elderly = cognitively unimpaired elderly; EOAD = early-onset Alzheimer's disease dementia; FTD = frontotemporal dementia; LOAD = late onset Alzheimer's disease dementia; NTPD = neurofibrillary tangle predominant dementia; Young = cognitively unimpaired young.

model was highly associated with CDR score ($P < 0.0001$, $R^2 = 0.73$), MMSE score ($P < 0.0001$, $R^2 = 0.51$), ^{18}F-AZD4694 SUVR ($P < 0.0001$, $R^2 = 0.53$), and hippocampal volume ($P < 0.0001$, $R^2 = 0.39$). In addition, Braak stages were associated with clinical diagnosis (cognitively unimpaired, MCI, Alzheimer's disease dementia) ($P < 0.0001$, $R^2 = 0.61$), amyloid-β status ($P < 0.0001$, $R^2 = 0.40$), and neurodegeneration status ($P < 0.0001$, $R^2 = 0.32$). Models that considered CDR score and amyloid-β status ($P < 0.0001$, $R^2 = 0.75$) or MMSE score and

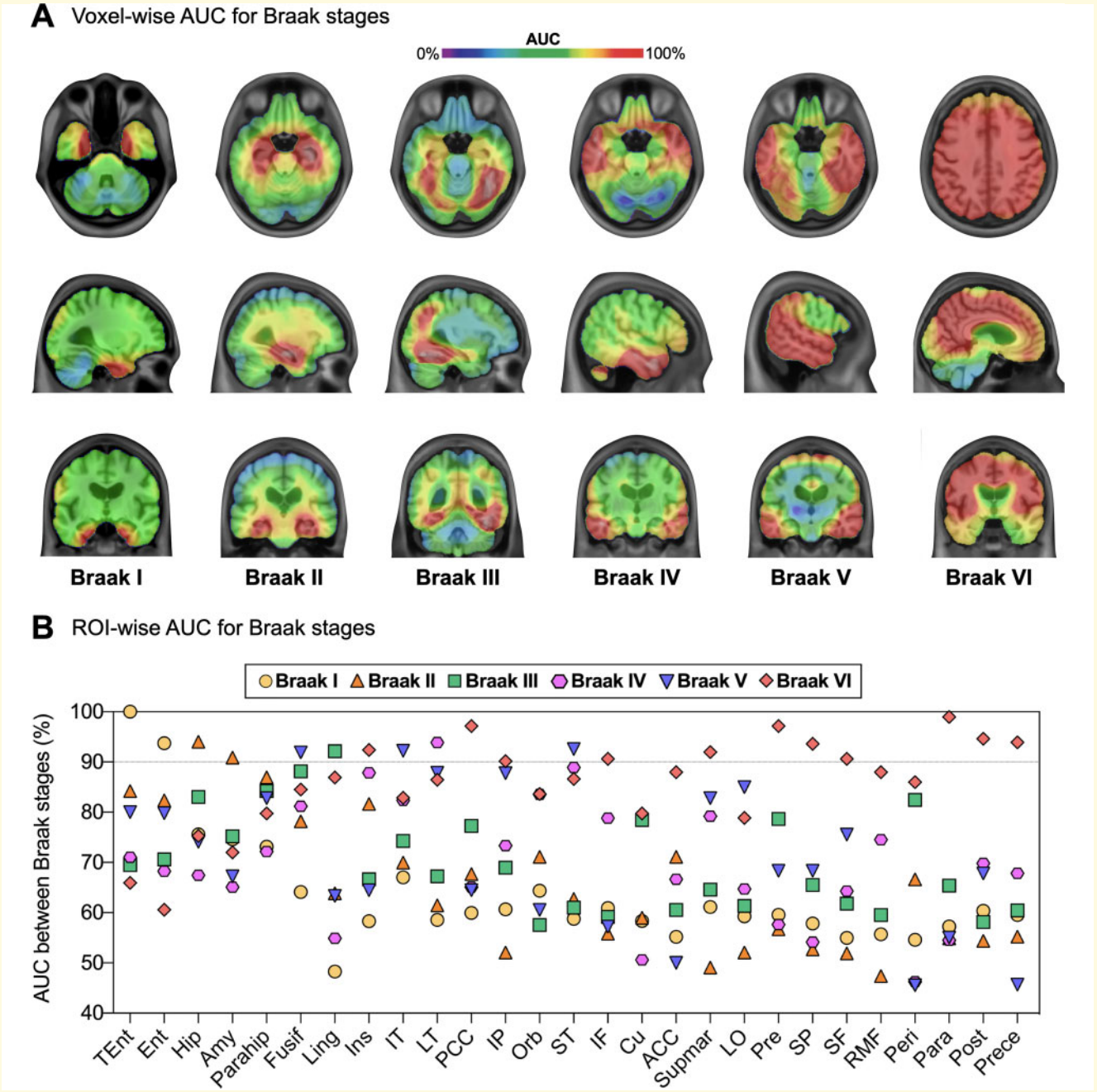

Figure 6 Receiver operating characteristic curve analysis reveals that no single brain region accurately segregated individuals across the six Braak stages. (**A**) From *left* to *right*: voxel-wise areas under the curve (AUC) maps for Braak I (contrasting Braak 0 versus Braak I), Braak II (Braak I versus Braak II), Braak III (Braak II versus Braak III), Braak IV (Braak III versus Braak IV), and Braak V (Braak IV versus Braak V), and Braak VI (Braak V versus Braak VI). (**B**) AUC in the anatomically segregated brain region reveals that no single brain region was able to accurately segregate individuals into the six Braak stages (yellow: AUC differentiating Braak 0 versus Braak I subjects), (orange: Braak I versus Braak II), (green: Braak II versus Braak III), (pink: Braak III versus Braak IV), (purple: Braak IV versus Braak V), (red: Braak V versus Braak VI). ACC = anterior cingulate; Amy = amygdala; Cu = cuneus; Ent = entorhinal; Fusif = fusiform gyrus; Hip = hippocampus; IF = inferior frontal; Ins = insula; IP = inferior parietal; IT = inferior temporal; Ling = lingual gyrus; LO = lateral occipital; LT = lateral temporal; Orb = orbitofrontal; Para = paracentral; Parahip = parahippocampal gyrus; PCC = posterior cingulate; Peri = pericalcarine; Post = postcentral; Pre = precuneus; Prece = precentral; RMF = rostro medial frontal; ROI = region of interest; SF = superior frontal; SP = superior parietal; ST = superior temporal; Supmar = supramarginal gyrus; TEnt = transentorhinal.

Table 2 Frequency of abnormal amyloid-β deposition, neurodegeneration, and cognition across Braak stages

Braak Stage	Amyloid-β deposition	Neurodegeneration	Cognitively unimpaired	Mild cognitive symptoms	Dementia
0	21%	11%	94%	6%	0%
I	43%	21%	86%	7%	7%
II	49%	22%	80%	14%	6%
III	77%	44%	66%	44%	0%
IV	85%	78%	43%	43%	14%
V	100%	75%	0%	50%	50%
VI	100%	77%	0%	23%	77%

The table shows the percentage of amyloid-β positivity and neurodegeneration abnormality, mild cognitive and dementia symptoms in individuals segregated by Braak stages across the Alzheimer's disease spectrum (cognitively unimpaired elderly, MCI amyloid-β+, and Alzheimer's disease amyloid-β+).

amyloid-β status ($P < 0.0001$, $R^2 = 0.66$) explained most of the Braak stages variance.

The combination of ^{18}F-MK-6240 Braak stages and amyloid-β ^{18}F-AZD4694 SUVR values separated Alzheimer's disease dementia versus cognitively unimpaired (amyloid-β plus Braak stages area under the curve = 98%, only amyloid-β area under the curve = 93%), Alzheimer's disease dementia versus MCI (amyloid-β plus Braak stages area under the curve = 86%, only amyloid-β area under the curve = 71%), Alzheimer's disease dementia versus frontotemporal dementia (amyloid-β plus Braak stages area under the curve = 100%, only amyloid-β area under the curve = 100%), MCI versus cognitively unimpaired (amyloid-β plus Braak stages area under the curve = 78%, only amyloid-β area under the curve = 78%), and MCI versus frontotemporal dementia (amyloid-β plus Braak stages area under the curve = 95%, only amyloid-β area under the curve = 92%) with high accuracy.

No single region of interest accurately segregates individuals into the six topographic Braak stages

Receiver operating characteristic curves analysis between Braak stages revealed that no single brain region was able to accurately segregate individuals in the six Braak stages (Fig. 6A and B). The brain regions in which SUVR values best represented each one of the Braak stages were the transentorhinal (Braak I), hippocampus (Braak II), lingual gyrus (Braak III), lateral temporal (Braak IV), superior temporal (Braak V), and paracentral gyrus (Braak VI) cortices (Fig. 6B).

Discussion

We found that ^{18}F-MK-6240 differentiates Alzheimer's disease from cognitively unimpaired and frontotemporal dementia with high accuracy. Furthermore, the distribution of ^{18}F-MK-6240 uptake *in vivo* recapitulated early and late Braak stages of neurofibrillary tangle deposition in preclinical and symptomatic individuals (Braak and Braak, 1991, 1997; Braak *et al.*, 2006, 2011). ^{18}F-MK-6240 Braak stages were closely related to amyloid-β status, neurodegeneration, and cognitive impairment; therefore, it shows the potential to be used as an index of tau accumulation and disease stages in living patients.

^{18}F-MK-6240 shows high performance for the diagnosis of Alzheimer's disease

^{18}F-MK-6240 showed high performance for the diagnosis of individuals across the Alzheimer's disease spectrum, including amyloid-β+ cognitively unimpaired, MCI, and dementia patients. Our frontotemporal dementia population—composed of patients with sporadic disease or mutations not associated with neurofibrillary tangles—showed negligible ^{18}F-MK-6240 uptake, supporting the specificity of ^{18}F-MK-6240 for tau tangle conformations. Similarly, previous studies have shown that tau PET discriminated Alzheimer's disease dementia from cognitively unimpaired elderly or other dementias with high accuracy (Ossenkoppele *et al.*, 2018). Although ^{18}F-MK-6240 showed accumulation in a high number of cognitively unimpaired elderly and MCI, the large difference in magnitude of ^{18}F-MK-6240 uptake between Alzheimer's disease dementia and cognitively unimpaired elderly and MCI allowed for separation of these populations with high accuracy. On the other hand, the amyloid-β deposition found in our non-dementia populations was similar in magnitude to that found in Alzheimer's disease dementia patients, which limits the performance of amyloid-β PET as a single biomarker for stage individuals across the Alzheimer's disease spectrum. Together, these findings support ^{18}F-MK-6240 tau tangle imaging as a highly sensitive and specific biomarker tool to contribute to the investigation of patients with suspected Alzheimer's disease pathophysiology.

^{18}F-MK-6240 accumulation in the absence of prominent amyloid-β pathology

We found numerous amyloid-β– individuals with abnormal ^{18}F-MK-6240 tau accumulation in brain regions comprising Braak stages I to IV, mostly confined to the temporal lobe. In our elderly population (cognitively unimpaired, MCI, and Alzheimer's disease), 82% of Braak 0, 65% of Braak I, 54% of Braak II, 30% of Braak III, and 14% of Braak IV cases were amyloid-β–. Post-mortem studies have also described neurofibrillary tangle accumulation in the absence of amyloid-β deposition mostly confined to the temporal cortex of the elderly (Braak and Braak, 1997; Braak *et al.*, 2011), which was named primary age-related tauopathy (Crary *et al.*, 2014). Together, our results indicate that primary age-related tauopathy with tau deposition confined to the temporal lobe is a common PET finding in the living elderly. On the other hand, the spread of tau tangles outside the temporal lobe has been generally associated with amyloid-β deposition (Price and Morris, 1999; Jagust, 2018; Villemagne *et al.*, 2018). Here, only 5/130 (4%) elderly amyloid-β– subjects had tau deposition in Braak V–VI regions, two were amnestic MCI and three had dementia symptoms indistinguishable from Alzheimer's disease. Thus, our results suggest the possibility of tau accumulation outside the temporal lobe without prominent amyloid-β deposition in a small percentage of the elderly, which may often be (3/5, 60%) associated with dementia symptoms clinically similar to those seen in Alzheimer's disease. We defined individuals with a clinical diagnosis of Alzheimer's disease dementia and *in vivo* PET suggesting high neocortical tau tangle load and scarce amyloid-β pathology, as patients with dementia with predominant neurofibrillary tangle pathology. However, it is important to emphasize that these results are derived from a small number of subjects and that these individuals may have amyloid-β pathology, but with unusually low concentrations for symptomatic patients with widespread tau accumulation.

^{18}F-MK-6240 accumulation recapitulates the six-stage Braak model

The vast majority of our participants (98%) had ^{18}F-MK-6240 tau tangle deposition consistent with the stereotypical patterns proposed by Braak in post-mortem cohorts, from the transentorhinal to primary sensory cortices (Braak and Braak, 1991). In the six individuals whose tau distribution diverged from the canonical Braak staging, five were consistent with the hippocampal sparing variant of Alzheimer's disease (Murray *et al.*, 2011). The aforementioned findings are similar to those previously reported using ^{18}F-flortaucipir (Schwarz *et al.*, 2016). On the other hand, we found that 37% of cognitively unimpaired amyloid-β– and 68% of cognitively unimpaired amyloid-β+ subjects were Braak stage I or higher using ^{18}F-MK6240, which contrasts with ∼10% and ∼30% of non-zero ^{18}F-flortaucipir Braak stages in cognitively unimpaired amyloid-β– and cognitively unimpaired amyloid-β+, respectively (Schwarz *et al.*, 2016; Pontecorvo *et al.*, 2017; Lowe *et al.*, 2018). Also, we showed that brain amyloid-β deposition and general cognitive performance explained most of the variance in ^{18}F-MK-6240 Braak stages. One may argue that the greater affinity of ^{18}F-MK-6240 to tau tangles compared to ^{18}F-flortaucipir is likely one of the reasons for the aforementioned differences in the results of these tracers (Hostetler *et al.*, 2016). The high sensitivity of ^{18}F-MK-6240 to tau tangles and the fact its Braak stages occurred in parallel to Alzheimer's disease pathophysiology support the use of ^{18}F-MK-6240 uptake to segregate living patients in early and late disease stages.

^{18}F-MK-6240 Braak staging applications in clinical and research settings

^{18}F-MK-6240 Braak stages could be used to stratify individuals with abnormal tau deposition in clinical and research settings. Although tau tangle deposition occurs naturally on a continuum, dichotomization into tau positive or negative groups is important for clinical diagnosis, population enrichment of clinical trials, and for assessing clinical changes associated with tau pathology (Gauthier *et al.*, 2016; Jack *et al.*, 2016). Our results suggest that the stratification of individuals into seven classes of tau accumulation (Braak 0–VI) can provide important information overlooked by dichotomization techniques. We demonstrated that, in the absence of any other biomarker in a clinical setting, patients in ^{18}F-MK-6240 Braak stage 0 could be associated with a low risk of amyloid-β pathology, neurodegeneration, and forthcoming cognitive impairment; Braak IV or greater with a high risk of underlying neurodegeneration; and Braak V–VI with likely imminent development of dementia symptoms. These results highlight that *in vivo* Braak staging using the novel high-affinity tau PET tracers can provide a more comprehensive evaluation of the significance of underlying tau deposition compared to mere dichotomization into tau positive and negative classes.

From a clinical trial perspective, one could predict that *in vivo* Braak staging can contribute to the interpretation of therapeutic effects on tau pathology over time. For instance, if an individual with baseline Braak II and an individual with baseline Braak V are enrolled in the same clinical trial and the posterior cingulate is used as the surrogate variable, it is likely that the Braak II individual will naturally have a lower rate of tau accumulation in this region than the Braak V individual, which needs to be taken into account to assess possible drug effects on these individuals. Thus, a clinical trial population enrichment using Braak stages would reduce the variability induced by inherently different regional rates

of tau deposition presented by individuals in different stages of tau accumulation. Thus, future anti-tau clinical trials could enrol individuals with a similar baseline Braak stage to minimize the bias introduced by the hierarchical accumulation of tau in the human brain cortex.

This study has methodological limitations. Although ^{18}F-MK-6240 has a high affinity to tau tangles, *in vivo* PET is likely to be less sensitive than neuropathological examination. The lower spatial resolution of PET compared to post-mortem analysis limits the delimitation of Braak stages in small regions as well as anatomical variations between subjects. Biomarkers provide naturally continuous measurements; therefore, thresholds are invariably affected by the method of analysis utilized. In addition, the lack of post-mortem data limits the interpretation of ^{18}F-MK-6240 SUVR cut-offs and Braak stages. Our population is composed of persons motivated to participate in a dementia study. Therefore, due to self-selection bias, these individuals may not represent the general population. Finally, we used a cross-sectional design to model the pathophysiological progression of Alzheimer's disease in individuals across the disease spectrum. Thus, it would be highly desirable to extrapolate our findings using longitudinal analysis.

To conclude, our results support that ^{18}F-MK-6240 Braak staging provides an index of tau deposition and disease stage with the potential to be incorporated in the diagnosis of living patients with suspected Alzheimer's disease pathophysiology.

Acknowledgements

The authors thank all participants of the study and staff of the McGill Center for studies in Aging. We thank Dean Jolly, Alexey Kostikov, Monica Samoila-Lactatus, Karen Ross, Mehdi Boudjemeline, and Sandy Li for assist in the radiochemistry production. We also thank Richard Strauss, Edith Strauss, Guylaine Gagne, Carley Mayhew, Tasha Vinet-Celluci, Karen Wan, Sarah Sbeiti, Meong Jin Joung, Miloudza Olmand, Rim Nazar, Hung-Hsin Hsiao, Reda Bouhachi, and Arturo Aliaga for consenting subjects and/or helping with data acquisition. We thank the Cerveau Technologies for the use of MK6240.

Funding

This research is supported by the Weston Brain Institute, Canadian Institutes of Health Research (CIHR) (MOP-11-51-31, FRN, 152985, PI: P.R-N.), the Alzheimer's Association (NIRG-12- 92090, NIRP-12-259245, P.R-N.), Fonds de Recherche du Québec – Santé (FRQS; Chercheur Boursier, P.R-N. and 2020-VICO-279314). P.R-N., S.G., and T.P. are members of the CIHR-CCNA Canadian Consortium of Neurodegeneration in Aging. Canada Foudation for innovation. Project 34874. CFI Project 34874.

Competing interests

The authors report no competing interests.

Supplementary material

Supplementary material is available at *Brain* online.

References

Alafuzoff I, Arzberger T, Al-Sarraj S, Bodi I, Bogdanovic N, Braak H, et al. Staging of neurofibrillary pathology in Alzheimer's disease: a study of the BrainNet Europe Consortium. Brain Pathol 2008; 18: 484–96.

Betthauser TJ, Cody KA, Zammit MD, Murali D, Converse AK, Barnhart TE, et al. In vivo characterization and quantification of neurofibrillary tau PET radioligand (18)F-MK-6240 in humans from alzheimer disease dementia to young controls. J Nucl Med 2019; 60: 93–9.

Betthauser TJ, Koscik RL, Jonaitis EM, Allison SL, Cody KA, Erickson CM, et al. Amyloid and tau imaging biomarkers explain cognitive decline from late middle-age. Brain 2020; 143: 320–35.

Braak H, Alafuzoff I, Arzberger T, Kretzschmar H, Del Tredici K. Staging of Alzheimer disease-associated neurofibrillary pathology using paraffin sections and immunocytochemistry. Acta Neuropathol 2006; 112: 389–404.

Braak H, Braak E. Neuropathological stageing of Alzheimer-related changes. Acta Neuropathol 1991; 82: 239–59.

Braak H, Braak E. Frequency of stages of Alzheimer-related lesions in different age categories. Neurobiol Aging 1997; 18: 351–7.

Braak H, Thal DR, Ghebremedhin E, Del Tredici K. Stages of the pathologic process in Alzheimer disease: age categories from 1 to 100 years. J Neuropathol Exp Neurol 2011; 70: 960–9.

Chien DT, Bahri S, Szardenings AK, Walsh JC, Mu F, Su MY, et al. Early clinical PET imaging results with the novel PHF-tau radioligand [F-18]-T807. J Alzheimers Dis 2013; 34: 457–68.

Crary JF, Trojanowski JQ, Schneider JA, Abisambra JF, Abner EL, Alafuzoff I, et al. Primary age-related tauopathy (PART): a common pathology associated with human aging. Acta Neuropathol 2014; 128: 755–66.

Cselenyi Z, Jonhagen ME, Forsberg A, Halldin C, Julin P, Schou M, et al. Clinical validation of 18F-AZD4694, an amyloid-beta-specific PET radioligand. J Nucl Med 2012; 53: 415–24.

Gauthier S, Feldman HH, Schneider LS, Wilcock GK, Frisoni GB, Hardlund JH, et al. Efficacy and safety of tau-aggregation inhibitor therapy in patients with mild or moderate Alzheimer's disease: a randomised, controlled, double-blind, parallel-arm, phase 3 trial. Lancet 2016; 388: 2873–84.

Gordon BA, Friedrichsen K, Brier M, Blazey T, Su Y, Christensen J, et al. The relationship between cerebrospinal fluid markers of Alzheimer pathology and positron emission tomography tau imaging. Brain 2016; 139: 2249–60.

Guillozet AL, Weintraub S, Mash DC, Mesulam MM. Neurofibrillary tangles, amyloid, and memory in aging and mild cognitive impairment. Arch Neurol 2003; 60: 729–36.

Harada R, Okamura N, Furumoto S, Furukawa K, Ishiki A, Tomita N, et al. 18[F]THK-5117 PET for assessing neurofibrillary pathology in Alzheimer's disease. Eur J Nucl Med Mol Imaging 2015; 42: 1052–61.

Heutink P. Untangling tau-related dementia. Hum Mol Genet 2000; 9: 979–86.

Hostetler ED, Walji AM, Zeng Z, Miller P, Bennacef I, Salinas C, et al. Preclinical characterization of 18F-MK-6240, a promising PET tracer for in vivo quantification of human neurofibrillary tangles. J Nucl Med 2016; 57: 1599–606.